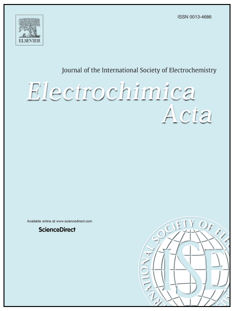
ISSN 0013-4686
ELSEVIER
Journal of the International Society of Electrochemistry
Electrochimica Acta
Available online at www.sciencedirect.com
ScienceDirect

Iron and cobalt hydroxides: Describing the oxygen evolution reaction activity trend with the amount of electrocatalyst

Javier Quiñonero, Roberto Gómez

PII: S0013-4686(18)30818-1
DOI: 10.1016/j.electacta.2018.04.074
Reference: EA 31641

To appear in: *Electrochimica Acta*

Received Date: 18 January 2018
Revised Date: 22 March 2018
Accepted Date: 10 April 2018

Please cite this article as: J. Quiñonero, R. Gómez, Iron and cobalt hydroxides: Describing the oxygen evolution reaction activity trend with the amount of electrocatalyst, *Electrochimica Acta* (2018), doi: 10.1016/j.electacta.2018.04.074.

This is a PDF file of an unedited manuscript that has been accepted for publication. As a service to our customers we are providing this early version of the manuscript. The manuscript will undergo copyediting, typesetting, and review of the resulting proof before it is published in its final form. Please note that during the production process errors may be discovered which could affect the content, and all legal disclaimers that apply to the journal pertain.

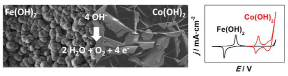
$Fe(OH)_2$
$4\ OH^-$
$2\ H_2O + O_2 + 4\ e^-$
$Co(OH)_2$
j / mA·cm^{-2}
$Co(OH)_2$
$Fe(OH)_2$
E / V

Iron and Cobalt Hydroxides: Describing the Oxygen Evolution Reaction Activity Trend with the Amount of Electrocatalyst

Javier Quiñonero, Roberto Gómez*

Departament de Química Física i Institut Universitari d'Electroquímica

Universitat d'Alacant, Apartat 99, E-03080 Alicante, Spain

*Corresponding author. Tel: +34 96 590 3748; email address: roberto.gomez@ua.es

Abstract

Although the amount of oxygen evolution electrocatalyst is a factor determining its efficiency, its fundamental correlation with activity remains unclear. To address this issue, we take advantage of a urea-based chemical bath deposition method (CBD) that enables to control the amount of electrocatalyst ($Fe(OH)_2$ and α-$Co(OH)_2$) deposited on conducting glass. The thickness of the resulting films, whose use in electrocatalysis is unprecedented, is tuned by controlling the deposition time. The turnover frequency (TOF) for O_2 generation decreases drastically as the electrocatalyst amount increases from equivalent coverages of 3.5 monolayers (ML) for $Fe(OH)_2$ and of 0.06 ML for α-$Co(OH)_2$ electrodes. The contrasting behavior of both hydroxides comes from the different structure of the incipient deposits, formed by small acicular nanoparticles in the case of $Fe(OH)_2$ and larger flat microparticles in the case of α-$Co(OH)_2$. The former structure allows a large fraction of the Fe sites to be in direct contact with solution, while such a fraction rapidly diminishes with loading for α-$Co(OH)_2$. In addition, the resulting $Co(OH)_2$ electrodes show TOFs similar or higher than those of electrodes prepared by more complex routes. The optimum ultrathin films are remarkably stable in

alkaline media, showing that the preparation of efficient electrocatalysts for oxygen evolution with an extremely small amount of metal through a novel, facile and scalable CBD is possible.

Keywords: iron hydroxide, cobalt hydroxide, chemical bath deposition, oxygen evolution reaction, electrocatalysis

1. Introduction

The electrolysis of water to produce oxygen and hydrogen is being considered as an attractive technology for sustainable and highly efficient energy generation [1–5]. The oxygen evolution reaction (OER), which is characterized by a slow kinetics (*i.e.*, large anodic overpotential) remains a critical step in this process and represents a significant efficiency loss in both electricity-driven and photodriven water splitting [6,7]. This fact prevents the straightforward development of certain clean energy technologies, including rechargeable metal-air batteries, water electrolysis systems, and solar-fuel devices.

Since the earliest works on OER electrocatalysis were reviewed by Trasatti [8,9] and Matsumoto [10] over thirty years ago, considerable research effort has been devoted to the design, synthesis, and characterization of efficient oxygen evolution catalysts (OECs). Currently, the optimal OECs in acidic media are noble metal-based catalysts, such as IrO_2 and RuO_2, since they exhibit the lowest overpotentials for the OER at practical current densities [11–14]. However, the scarcity of the corresponding metals, high cost, and poor long-term stability in alkaline media have hindered large-scale applications and highlighted the need for OECs with prospects of being employed at a practical level.

In this context, several studies have revealed that first-row transition metal oxides and (oxy)hydroxides (Mn [15–17], Fe [18–20], Co [21–23], and Ni [24–26]), along with certain spinel [27–29] and perovskite oxides [30–32], could offer a compromise solution: although they possess nonoptimal OER electrocatalytic activity, their environmental friendliness, low cost, and abundance in nature convert them into practical candidates for OECs [33–35]. In addition, they are stable in neutral to alkaline solutions and display moderate to good electrical conductivities. However, due to the existence of polymorphs, incidental impurity incorporation, and complicating effects of electronic conductivity and electrochemically active surface area, the fundamental correlations of activity to structure, composition, and amount of electrocatalyst are not quantitatively described.

In any case, iron-group metal hydroxides ($Fe(OH)_2$, $Co(OH)_2$ and $Ni(OH)_2$) with a layered structure have been suggested to be active, stable, and inexpensive electrocatalysts for OER. In fact, it has been reported that, analogously to the already extensively described $NiOOH/Ni(OH)_2$ system [36,37], cobalt hydroxide ($Co(OH)_2$) crystallizes in two polymorphs (α- and β-$Co(OH)_2$), which can be oxidized to γ- and β-CoOOH, respectively [38]. Although both hydroxides have been found able to efficiently catalyze OER [21,39], recent studies indicate that α-$Co(OH)_2$ shows better performance than β-$Co(OH)_2$, regardless of particle size or surface area [40]. This has motivated the search for synthesis methods able to stabilize the alpha form of the material for its application as OEC. On the other hand, due to the Fe high abundance and non-toxicity, $Fe(OH)_2$-based OECs are also appealing [41], although they have been considered to have poor OER activity due to the intrinsic low electronic conductivity and relative instability of the oxidized form (γ-FeOOH) [42]. In any case, the interest of its study as an OEC lies in the fact that the incorporation of Fe impurities into $Ni(OH)_2$-

[43,44] and $Co(OH)_2$-based [45] OECs has been found to lead to an enhancement of their electrocatalytic performance. These observations have promoted the development of double hydroxide systems (such as Ni-Fe [46–48], Ni-Co [49,50], and Co-Fe [45]), facilitated by the capacity of iron-group transition metals of presenting different oxidation states and coordination environments. Interestingly, they have indeed exhibited enhanced OER activity compared to monometallic hydroxide systems.

In this work, ultrathin $Fe(OH)_2$ and α-$Co(OH)_2$ films have been deposited on $F{:}SnO_2$ (FTO) conducting glass substrates by a urea-based chemical bath deposition (CBD) method. To the best of our knowledge, such a method is applied for the first time to prepare $Fe(OH)_2$ ultrathin films, while it has been previously employed for preparing supercapacitor electrodes in the case of α-$Co(OH)_2$ [51,52]. As far as we know, α-$Co(OH)_2$ ultrathin films prepared in this way are tested as electrocatalysts for the first time. The CBD method, apart from being inexpensive, scalable and extremely versatile, is especially advantageous over other synthetic procedures (hydrothermal, electrodeposition, co-precipitation…) as it offers the possibility of finely tuning the deposited amount of $Fe(OH)_2$ and $Co(OH)_2$ by only controlling the deposition time while directly achieving a catalyst thin film with a well-defined morphology. In such a way, electrodes with different deposited amounts of $Fe(OH)_2$ and $Co(OH)_2$ have been synthesized and their electrocatalytic activity toward the OER has been studied in alkaline media. Remarkably, low amounts of Fe and, particularly, of Co (well below the monolayer) are required for the best OER performance. This type of study allows us to approach the design of double-hydroxide structures with controlled composition, which can result in a completely tunable and improved OER behavior. It is also remarkable that these electrodes are highly transparent, which is of great importance for their potential application in photoelectrochemical devices (i.e., water splitting cells).

2. Experimental section.

2.1. Preparation of $Fe(OH)_2$ and α-$Co(OH)_2$ electrodes. $Fe(OH)_2$ and α-$Co(OH)_2$ were deposited on fluorine-doped tin oxide ($F:SnO_2$, FTO, U-type 12 Ω·□, Asahi Glass Co.) substrates by a CBD procedure [25]. The deposition solution contained 25 mL of 0.5 M $FeSO_4 \cdot 7H_2O$ (Sigma-Aldrich, 99%) or $CoSO_4 \cdot 7H_2O$ (Sigma-Aldrich, 99%), for the deposition of $Fe(OH)_2$ or α-$Co(OH)_2$, respectively, 12.5 mL of 1 M urea (Sigma-Aldrich, P.A.) and 12.5 mL of H_2O (Millipore, Essential Elix 3). FTO glass plates were cleaned by 15-min sonication (Selecta Ultrasonics) in acetone (Panreac, P.A.) and ethanol (VWR Prolabo Chemicals, 96%) and, then, vertically supported with the conducting side faced against the wall of the beaker containing the CBD solution. The area of FTO substrate to be covered with the hydroxide deposit was, approximately, of 1 cm^2. The solution was heated up to 100ºC in a stove (Memmert, 100-800). Different deposition times (from 2.5 min to 2.5 h) were assayed as to control the amount of deposited metallic hydroxide. After deposition, the samples were rinsed with distilled water, air-dried and, in the case of $Fe(OH)_2$ deposits, annealed at 200ºC in air for 1 h (Conatec, 7800) with a heating rate of $5ºC \cdot min^{-1}$.

2.2. Electrode characterization and electrochemical measurements. Electrochemical measurements were conducted at room temperature in a home-made Pyrex glass cell and a computer-controlled potentiostat-galvanostat (Autolab, PGSTAT30). A Pt wire and an Ag/AgCl/KCl(3 M) electrode were used as counter and reference electrodes, respectively. All potentials are referred to the Ag/AgCl electrode unless otherwise stated. An N_2-purged 1 M NaOH solution was used as the working electrolyte for the electrochemical measurements.

The crystal structure of $Fe(OH)_2$ and α-$Co(OH)_2$ deposits were identified by XRD (Bruker D8-Advance, using Cu Kα radiation) with the rotatory anode operating at 40 kV and 40 mA, and with a step scan of 0.5º·min^{-1}. Raman spectra were obtained with a laser Raman spectrometer (Jasco, NRS–5100), using an excitation line provided by an Ar laser at 531.92 nm. To elucidate the surface chemical composition along with the valence states of the elements present in the films, XPS experiments were performed with a Thermo-Scientific K-Alpha XPS spectrometer equipped with a monochromatic Al-Kα source (1486.6 eV), operating at 15 kV and 10 mA. A SEM study was carried out to characterize the surface morphology of the films using a ZEISS Merlin VP Compact field emission scanning electron microscope (FESEM). The optical properties of the α-$Co(OH)_2$ films before and after their electrochemical characterization were studied by solid-state UV-vis spectroscopy, using a Shimadzu UV-2401 PC spectrophotometer working in the absorbance mode.

3. Results and discussion.

3.1. $Fe(OH)_2$ electrodes. Figure 1a shows the XRD patterns for an FTO conductive glass substrate prior and after the deposition of $Fe(OH)_2$ (for a deposition time of 2.5 hours). Apart from FTO, $Fe(OH)_2$ is the only crystalline phase detected in the film (PDF file: 13-0089). The XRD analysis confirms that the slightly brown $Fe(OH)_2$ films are crystalline, presenting a hexagonal phase, with the following lattice parameters: $a = b = 3.258$ Å, $c = 4.605$ Å, $\alpha = \beta = 90º$ and $\gamma = 120º$. In addition, the Raman spectrum corresponding to the as-synthesized $Fe(OH)_2$ (Figure S1) agrees with that reported in the literature for this crystalline phase [53]. Figure 1b and 1c contains XPS spectra of the $Fe(OH)_2$ sample prepared for a deposition time of 2.5 hours. The XPS spectrum for Fe 2p (Fig. 1b) shows two main peaks with binding energies (BE) of 711.0 eV and 724.9 eV, corresponding to the Fe $2p_{3/2}$ and $2p_{1/2}$ transitions, respectively, while the two peaks with lower intensity at BE of 715.9 eV and 733.3 eV can be identified as satellite peaks. This complex but characteristic multiplet splitting, along with the presence of satellite features, indicate the existence of Fe^{2+} species in a high-spin environment [54,55]. This fact and the observed O 1*s* transition with a BE of 531.0 eV (Fig. 1c) associated with the existence of hydroxide groups [56], provide evidence that the as-prepared samples are entirely composed of $Fe(OH)_2$. Representative top FESEM images of $Fe(OH)_2$ samples with deposition times of 20 min and 2.5 hours are shown in Figure 1d and 1e, respectively. Figure S2 shows FESEM images of $Fe(OH)_2$ deposits on FTO substrates for deposition times of 10, 30 and 40 min. As observed in Figures 1d and S1, the chemical bath deposition procedure induces the formation of a clear over-structure on the relatively rough surface of the FTO substrate. It is composed of very fine grains that, at early stages of the $Fe(OH)_2$ deposition process, seem to grow homogeneously distributed only on certain faces of the substrate. Insets in Figure S2 also provide a representative picture of the bare FTO substrate, whose roughness factor (the ratio of the real surface area evaluated from the FESEM image and the corresponding plane-projected area) can be estimated as 3.7. For longer deposition times (Figure 1e), the $Fe(OH)_2$ deposit significantly grows, covering all the FTO substrate and giving rise to a deposit with a better developed morphology constituted by slightly rough, rounded particles of around 100-150 nm of diameter.

Figure 2 shows cyclic voltammograms for FTO/$Fe(OH)_2$ electrodes prepared for different deposition times together with a blank voltammogram for the bare FTO substrate Figure S3 show cyclic voltammograms for FTO/$Fe(OH)_2$ electrodes prepared for deposition times of 60, 90 and 120 min, together with the corresponding FESEM images. As $Fe(OH)_2$ deposition proceeds, a quasi-reversible couple of peaks grows between -1.1 and -0.7 V, which is associated with the redox process (Eq. 1):

$$\mathrm{Fe(OH)_2 + OH^- \leftrightarrows FeOOH + H_2O + e^-} \qquad \text{Eq. (1)}$$

Importantly, similar quasi-reversible electrochemical behavior is observed for both incipient and relatively thick $Fe(OH)_2$ films. Such a high degree of definition in the electrochemical response suggests that the Fe sites in the sample are equivalent. The XRD pattern for a $Fe(OH)_2$ film (deposition time of 2.5 hours) after its electrochemical characterization (Figure S4) confirms the stability of the sample.

The deposition of $Fe(OH)_2$ on FTO has also a direct effect on the electrochemical behavior of these electrodes in the region of positive potentials (see inset in Figure 2). In fact, at potentials above 0.5 V, appreciable currents attributable to oxygen evolution are observed. The evolution of O_2 on the bare FTO substrate is negligible with respect to that of FTO/$Fe(OH)_2$ electrodes. The inset in Figure 2 clearly reveals that, although the charge associated with Fe oxidation (q_{Fe}) increases with the $Fe(OH)_2$ deposition time, the rate of O_2 generation is not following this trend. In fact, at 0.7 V, the current density observed for the 60-min deposit is higher than that of the 80-min deposit.

These results indicate that the O_2 generation rate is not simply proportional to the quantity of deposited $Fe(OH)_2$, but rather depends on the physical and morphological characteristics of the $Fe(OH)_2$ deposit (such as particle size, crystal structure, dispersion of the deposited particles, etc.). In this work, the electrocatalytic activity is defined as the current density for O_2 evolution (j_{OER}) at 0.7 V (that is, for an overpotential of 470 mV). Figure 3a shows a plot of the electrocatalytic activity with respect to the charge density corresponding to the oxidation of $Fe(OH)_2$ to FeOOH, which is obtained by integration of the corresponding voltammetric anodic peak as it is free of the interference from the O_2 reduction wave that affects the cathodic peak. Such a plot is explicitly representing how the electrocatalytic activity varies as a function of the amount of Fe, which, in turn, is dependent on the deposition time. As the charge density corresponding to the $Fe(OH)_2$ oxidation peak (proportional to the amount of deposited

$Fe(OH)_2$) increases up to 1.3 mC·cm^{-2}, the electrocatalytic activity rapidly grows until a plateau is reached. Beyond this point, no further improvement of the electrocatalytic activity is observed until an amount of deposited $Fe(OH)_2$ equivalent to 8 mC·cm^{-2} is reached. From this point, the electrocatalytic activity begins to progressively decrease with increasing $Fe(OH)_2$ oxidation charge densities.

It is worth noting that the electrocatalytic activity defined above is not a measure of the specific electrocatalytic ability of the system. Such a magnitude can be expressed in terms of the turnover frequency (TOF), defined here as the number of oxygen molecules generated at 0.7 V per second and per metallic atom (here, Fe) atom (Eq. 2) [25]:

$$\mathrm{TOF} = \frac{1}{N_{\mathrm{Fe}}} \cdot \frac{dN_{\mathrm{O_2}}}{dt} = \frac{1}{4} \cdot \frac{j_{0.7\,\mathrm{V}}}{q_{\mathrm{Fe}}} \qquad \text{Eq. (2)}$$

where q_{Fe} is the charge density corresponding to the oxidation of $Fe(OH)_2$ to FeOOH. The metallic centers are thus considered as being the catalytic sites the according to recent literature [57,58]. In fact, for first-row transition-metal (primarily, Mn, Fe, Co and Ni) oxides and (oxy)hydroxides as electrocatalysts for the OER, it is widely accepted that the process occurs on surface metal sites (M), via a series of adsorbed intermediates (*e.g.*, M–OH, M–O, M–OOH, M–OO).

Figure 3b shows a log-log plot of the TOF as a function of the $Fe(OH)_2$ charge density exchanged during the $Fe(OH)_2$ oxidation as determined from the corresponding cyclic voltammogram. The observed behavior indicates that the electrocatalyst loading is an important factor governing its electrocatalytic activity. In fact, TOF remains almost constant for values of deposited $Fe(OH)_2$ below 1 mC·cm^{-2}, and, beyond this point, increasing amounts of $Fe(OH)_2$ trigger a sharp decrease in the TOF values.

3.2. α-$Co(OH)_2$ electrodes. Figure 4a shows the XRD patterns for an FTO conductive glass substrate prior and after the deposition of $Co(OH)_2$ (for a deposition time of 2.5 hours). The XRD analysis confirms that the resulting blue films are crystalline *α*-

$Co(OH)_2$ (PDF file: 02-0925). It is important to mention that the main difference between the present XRD pattern and those usually reported is that the (003) diffraction peak at 9.6º (the most intense diffraction peak according to the literature [40,59,60]) is very weak relative to the other peaks. In this regard, Hu and coworkers [61] observed that the diffraction pattern corresponding to α-$Co(OH)_2$ containing intercalated SO_4^{2-} anions (which may be the case here according to the Co precursor employed in this synthesis) displays a considerable decrease in the intensity of the diffraction peaks when compared with α-$Co(OH)_2$ containing other intercalated anions (such as Cl^- or NO_3^-). This fact, together with the preferential orientation of the as-synthesized $Co(OH)_2$ films for long deposition times (see FESEM image below), could explain the significant variations in the relative intensities of the different diffraction peaks observed here. Raman spectra for the as-synthesized α-$Co(OH)_2$ (Figure S5) provides further evidence that the films are entirely made of crystalline $Co(OH)_2$ [52,62].

Figure 4b-c contains XPS spectra of the α-$Co(OH)_2$ sample obtained for a deposition time of 2.5 hours. As seen in Figure 4b, the XPS spectrum of Co 2*p* is characterized by the existence of two spin-orbit components corresponding to the Co $2p_{3/2}$ and $2p_{1/2}$ transitions at BE of 779.9 eV and 795.0 eV, respectively. The relatively intense satellite peaks at 789.8 eV and 804.2 eV also provide strong evidence that the Co species present in the as-prepared samples are in the form of Co^{2+} [63–65]. In addition, the binding energies of the main Co 2*p* contributions are separated by 15.1 eV, which is fully consistent with the reported value of the Co $2p_{3/2}$-$2p_{1/2}$ splitting for $Co(OH)_2$ [66,67]. These facts, along with the observed O 1*s* transition with a BE of 531.2 eV (Fig. 4c), indicate that the as-prepared samples are composed of $Co(OH)_2$, not surprisingly on the basis of the XRD data presented above [56]. Figure 4d-e displays FESEM images corresponding to α-$Co(OH)_2$ films for deposition times of 20 min and 2.5 hours, respectively. From Figure 4d, it can be deduced that the initial stages of the $Co(OH)_2$ deposition process on FTO proceed are slower than for $Fe(OH)_2$. In fact, no clear over-structure on the surface of the FTO substrate, attributable to the $Co(OH)_2$ formation, can be identified for deposition times of 40 min and below (see Figure S6). This indicates that the $Co(OH)_2$ amounts deposited for these times are extremely low. On the contrary, Figure 4e reveals a developed $Co(OH)_2$ morphology constituted by vertically oriented platelet structures of relatively large dimensions.

Figure 5 shows cyclic voltammograms for FTO/$Co(OH)_2$ electrodes prepared for different deposition times together with a blank voltammogram for the bare FTO substrate. Figure S7 show cyclic voltammograms for FTO/$Co(OH)_2$ electrodes prepared for deposition times of 60, 90 and 120 min, together with the corresponding FESEM images. The voltammograms for $Co(OH)_2$ films are characterized by the presence of two pairs of redox peaks, A_1/C_1 and A_2/C_2, located at about 0.05 and 0.40 V, respectively, in agreement with those reported in the literature for α-$Co(OH)_2$ electrocatalysts [68,69]. The redox peaks A_1/C_1 and A_2/C_2, whose areas increase as $Co(OH)_2$ deposition proceeds, can be assigned to the Co(III)/Co(II) and Co(IV)/Co(III) redox processes according to equations (3) and (4), respectively:

$$\mathrm{Co(OH)_2 + OH^- \leftrightarrows CoOOH + H_2O + e^-} \qquad \text{Eq. (3)}$$

$$\mathrm{CoOOH + OH^- \leftrightarrows CoO_2 + H_2O + e^-} \qquad \text{Eq. (4)}$$

It is remarkable that this reversible electrochemical behavior is observed from the second voltammetric cycle. On the contrary, the first one shows a highly irreversible oxidation peak between 0.0 and 0.5 V, especially for thick $Co(OH)_2$ films (Figure S8a). The charge density corresponding to the oxidation of $Co(OH)_2$ to CoOOH in the first voltammetric scan provides information about the total deposited $Co(OH)_2$ quantity (q_{Co}^{total}), while that corresponding to the same process in the second and following voltammetric cycles reveals the amount of electroactive $Co(OH)_2$ actually involved in the reversible redox process (q_{Co}^{rev}). Figure 6 shows a log-log plot of the $q_{Co}^{rev}/q_{Co}^{total}$ ratio as a function of q_{Co}^{total}, measured for FTO/Co(OH)$_2$ electrodes prepared for different deposition times. In this regard, as observed, incipient deposits show a more reversible electrochemical behavior than thicker films (Figure S8b). This electrochemical irreversibility of thicker Co(OH)$_2$ deposits is also revealed at a visual level. In fact, the initially blue-colored Co(OH)$_2$ deposits become dark brown/black after the first voltammetric cycle (Figure S9), and do not recover their initial blue coloration in successive voltammetric cycles. The XPS spectra for Co 2p and O 1s corresponding to an α-Co(OH)$_2$ sample obtained for a deposition time of 2.5 hours after its electrochemical characterization, suggests the existence of Co^{3+} and O^{2-} species (Figure S10). In any case, the corresponding XRD pattern after the electrochemical characterization (Figure S11) reveals that this electrochemical treatment does not alter the crystalline structure of the films, demonstrating the stability of the α-Co(OH)$_2$ samples.

As previously described for FTO/Fe(OH)$_2$ electrodes, the deposition of Co(OH)$_2$ on the FTO surface also has a direct effect on the electrochemical behavior of these electrodes in the region of positive potentials (higher than 0.55 V). In fact, at potentials immediately above the peak for CoOOH oxidation (A$_2$), significant currents attributable to oxygen evolution are observed. Figure 7a shows a plot of the electrocatalytic activity with respect to the charge density corresponding to the oxidation of Co(OH)$_2$ to CoOOH, which is obtained by integration of the corresponding voltammetric anodic peak (A$_1$). Once again, it is revealed that the rate of O$_2$ generation is not directly proportional to the amount of Co active sites. In this case, as the charge density corresponding to the Co(OH)$_2$ oxidation peak begins to increase, the electrocatalytic activity rapidly grows until a j_{OER} value of approximately 3.5 mA·cm^{-2} is reached. From this point forward, the electrocatalytic activity continues to grow, but now in a slower way. The resulting negative slope in the corresponding log-log plot of the TOF as a function of the charge density exchanged in the $Co(OH)_2$ oxidation (Fig. 7b) shows that TOF values are almost inversely proportional to the density of active $Co(OH)_2$ sites. Unlike the $Fe(OH)_2$ electrodes, the TOF for $Co(OH)_2$ only exhibits an approximately constant value for very small charge densities (small amounts of deposited electrocatalyst), showing afterward a marked decrease. Actually, TOF values start to decrease for a charge of the order of 10 $\mu A \cdot cm^{-2}$, roughly corresponding to one tenth of a ML for an atomically flat surface.

Although the different synthesis procedures and measurement conditions found in the literature hamper straightforward comparisons, it is remarkable that the results obtained for the OER electrocatalytic activity of α-$Co(OH)_2$ electrodes (in absolute terms of overpotential for a given current density value) are in the range typically reported in the literature. The overpotentials (η) needed for achieving a current density of 5 $mA \cdot cm^{-2}$ have values of 470 and 350 mV for an electrode with 30 and 90 $mC \cdot cm^{-2}$ of reversible Co, respectively. It is remarkable that, for a layered $Co(OH)_2$ nanosheet electrode on a glassy carbon substrate, Song and coworkers [70] achieved a density current of 5 $mA \cdot cm^{-2}$ for an overpotential of 340 mV, similar to that obtained here. In other studies, the required overpotentials to obtain such a current density value (5 $mA \cdot cm^{-2}$) were of 450 mV (for a CoOOH deposit on a Pt substrate [42]) and 360 mV (for an electrode made of α-$Co(OH)_2$ particles deposited on a glassy carbon substrate [71]). Therefore, the electrodes prepared by simple CBD on conducting glass offer similar results in terms of electrocatalytic performance to those reported for electrodes synthesized through more complex procedures [42,70,71]. This highlights the convenience of this method in the preparation of hydroxides for electrocatalytic applications. TOF values obtained here are also comparable to those in the literature. In fact, for the same layered $Co(OH)_2$ electrodes mentioned above, Song and coworkers [70] calculated a TOF value from the density current at η = 300 mV lower than 0.01 s^{-1}. Our results show that this TOF value (also at η = 300 mV) would correspond to a charge density of the order of 100 $mC \cdot cm^{-2}$. For lower values of charge density (on the order of 0.01, 0.1, 1 and 10 $mC \cdot cm^{-2}$), and in the same overpotential conditions, higher TOF values equivalent to 0.06, 0.08, 0.02 and 0.02 s^{-1}, respectively, are calculated.

A comparison of the results shown above reveals significant differences between $Fe(OH)_2$ and $Co(OH)_2$ at different levels. As previously commented, from the FESEM images obtained for FTO/$Fe(OH)_2$ and FTO/α-$Co(OH)_2$ electrodes for the same deposition times, it is evident that the $Co(OH)_2$ deposition on FTO is much slower than that of $Fe(OH)_2$. In fact, for deposition times of 40 min and below, the coverage degree of FTO substrates with $Fe(OH)_2$ is much higher than with α-$Co(OH)_2$. Without considering possible processes of complexation that can stabilize the metallic cations (Fe^{2+} and Co^{2+}) in solution and thus influence the precipitation reaction, this fact could be rationalized by considering the values of the solubility products (K_{ps}) for both metal hydroxides. At T = 25ºC, K_{ps} values for $Fe(OH)_2$ and α-$Co(OH)_2$ are $4.87 \cdot 10^{-17}$ and $5.92 \cdot 10^{-15}$, respectively [72]. In this way, Fe^{2+} cations would be more likely to precipitate in the form of hydroxide than Co^{2+} because of the slow alkalinization occurring during the hydrolysis of urea.

Apart from this, important differences in the electrocatalytic properties of $Fe(OH)_2$ and $Co(OH)_2$ for OER in alkaline media are observed. In fact, for equivalent charge densities for the oxidation of $M(OH)_2$ to MOOH (M: Fe or Co), the current densities attributable to OER for FTO/$Co(OH)_2$ electrodes are around 4 orders of magnitude higher than those corresponding to FTO/$Fe(OH)_2$ electrodes. This significant lower

OER activity of the FeOOH/$Fe(OH)_2$ system compared to the iron-group metals (oxy)hydroxides has been previously reported in the literature. Subbaraman and co-workers [42] deposited near-monolayer (oxy)hydroxide films on Pt single crystals and found activities of NiO_xH_y > CoO_xH_y > FeO_xH_y, which was correlated with the oxophilicity of the metal (*i. e.*, M–O bond strength). In this regard, Fe (oxy)hydroxide is considered to have the less-optimal M–O bond strength of the iron-group metals. These observations also coincide with the results corresponding to the iron-group metal oxides as OER catalysts. Trasatti [9] correlated the enthalpy of the reaction $MO_x + {}^1/_2\ O_2 \rightarrow MO_{x+1}$ (which could reasonably be correlated with the strength of the M–O bond) to the OER activity to generate a volcano relation where the iron-group metal oxides are in the order NiO > Co_3O_4 >> Fe_3O_4. In relation to this, Lyons and co-workers [73] studied electrochemically conditioned metal electrodes and found an activity trend of Ni > Co > Fe.

Fig. 8 shows the quasi-steady-state polarization curve for OER recorded for FTO/$Fe(OH)_2$ and FTO/$Co(OH)_2$ electrodes showing high electrocatalytic activity (in TOF terms). The Tafel slopes can be estimated to be 30 $mV\cdot dec^{-1}$ and 27 $mV\cdot dec^{-1}$, respectively. Consequently, the corresponding exchange current density value for the FTO/$Co(OH)_2$ electrode would be orders of magnitude higher than that corresponding to FTO/$Fe(OH)_2$, which supports the observations regarding the superior electrocatalytic behavior toward OER of α-$Co(OH)_2$ compared to $Fe(OH)_2$

The values of TOF obtained for FTO/$Fe(OH)_2$ and FTO/$Co(OH)_2$ electrodes (and also for FTO/$Ni(OH)_2$ electrodes, previously characterized as OECs in our laboratory [25]) for different amounts of deposited electrocatalyst also confirm these observations about the differences in OER activities. In the case of FTO/$Fe(OH)_2$ electrodes, the higher electrocatalytic activity (in TOF terms) remains constant for charge densities for the

$Fe(OH)_2$ oxidation lower than 1 $mC\cdot cm^{-2}$, which, according to previous studies [25], would be equivalent to a coverage of around 3.5 ML. This fact suggests that, as the $Fe(OH)_2$ electrical conductivity is extremely low, only the Fe(II) species in close vicinity to the conducting substrate and/or directly exposed to solution would catalyze the OER. In fact, for a few monolayer coverages and below (corresponding to the best TOF values), most of the iron atoms should be in isolated and columnar islands able to quickly exchange electrons with the conducting substrate, facilitating their role as electrocatalysts (Fig. 9a). As coverage grows (charge densities higher than 1 $mC\cdot cm^{-2}$), an increasing fraction of Fe atoms are in inner $Fe(OH)_2$ regions, depending for their functioning as catalytic centers on charge transport through the non-porous iron hydroxide layer, with the corresponding progressive decrease of TOF values. It is also apparent that the fraction of iron atoms exposed to the electrolyte (those active in electrocatalysis) will be maximum as the amount of deposited catalyst is minimized.

Similar considerations could be invoked to explain the TOF trend for FTO/α-$Co(OH)_2$ electrodes. The drastic decrease in TOF values with increasing amounts of deposited $Co(OH)_2$ suggests that the morphology of the film (*i. e.*, the average size of the incipient islands/nanoplatelets as well as their dispersion on the substrate) is an important factor governing its electrocatalytic activity. As the conductivity of $Co(OH)_2$ is rather low (but higher than that corresponding to $Fe(OH)_2$), the part of the film in direct contact with the conductive substrate and/or exposed to the electrolyte would contribute the most in the redox processes that give rise to the OER electrocatalytic activity of $Co(OH)_2$ (Fig. 9b). In addition, large amounts of deposited $Co(OH)_2$ lead to substantial electrochemical irreversible processes and the affected Co centers would not participate in the electrocatalytic process: the Co sites far away from the conducting substrate and not in direct contact with the electrolyte would remain in their oxidized form (Co^{3+}), being inactive in the OER process. Actually, it may be estimated that all the $Co(OH)_2$ films with a TOF higher than 1 s^{-1} are submonolayer deposits. In fact, the maximum value of TOF (around 30 s^{-1}) corresponds to a charge density of the order of 0.010 $mC \cdot cm^{-2}$, which is equivalent to a coverage of only 0.06 ML. Despite this, it is worth noting that, for the thicker $Co(OH)_2$ films, the oxygen generation currents continue to grow, probably due to the large open voids in the structure of the $Co(OH)_2$ film, which facilitates its efficient interaction with the electrolyte. In any case, it is important to remark that the fraction of $Fe(OH)_2$ or $Co(OH)_2$ films that can fully promote the OER electrocatalysis is presumably that in direct contact with the electrolyte and with the FTO substrate. This aspect highlights the need to maximize the interfacial area of the deposit with the aim of enhancing its electrocatalytic activity as a larger fraction of electrocatalyst would be directly exposed to solution and would thus be electrocatalytic active.

The comparison of the results regarding TOF values for $Fe(OH)_2$ and α-$Co(OH)_2$ electrodes with those corresponding to a widely described electrocatalyst such as the $NiOOH/Ni(OH)_2$ system may help put them in context. In a previous study [25], in which controlled amounts of $Ni(OH)_2$ were deposited on FTO by means of a chemical bath deposition method analogous to that employed now, a TOF value close to 30 s^{-1} (for a potential of 0.7 V) was calculated for only 10 $\mu C \cdot cm^{-2}$ of deposited $Ni(OH)_2$. For the same charge density and potential, the TOF values obtained for α-$Co(OH)_2$ and $Fe(OH)_2$ were of around 20 and 0.4 s^{-1}, respectively. The higher TOF values of $Ni(OH)_2$ compared to those corresponding to $Fe(OH)_2$ and $Co(OH)_2$ are probably linked to the superior OER activity that characterizes $Ni(OH)_2$ as an electrocatalyst.

Finally, we should emphasize that the coverage calculation for both types of electrodes has been done by assuming that the surface is perfectly flat, which is not the case. In fact, as we have estimated a roughness factor of around 3.7 for the FTO substrate, the actual number of equivalent monolayers calculated on the basis of the real surface area would be substantially lower.

4. Conclusions.

Ultrathin films of $Fe(OH)_2$ and α-$Co(OH)_2$ have been deposited on FTO substrates by means of a chemical bath deposition method, which is presented as a novel procedure to synthesize $Fe(OH)_2$ and $Co(OH)_2$ electrocatalysts in the form of thin films. In the case of $Co(OH)_2$ electrodes, the advantages of the CBD method with respect to other more complex synthetic procedures reported in the literature are especially evident as it leads to the polymorph with the highest electrocatalytic activity toward the OER (the α-$Co(OH)_2$ phase) without the need for a subsequent heat treatment. Interestingly, the performance of CBD-prepared α-$Co(OH)_2$ electrodes is comparable to the best results reported in the literature, achieved with electrodes prepared through more intricate synthesis procedures. It is also worth noting that these anodes are highly transparent, which is of great importance in the design of photoelectrochemical devices (such as water splitting ones), for instance when these metallic hydroxides are considered as possible efficient co-catalysts able to promote oxygen evolution.

By controlling the deposition time, samples with different $Fe(OH)_2$ and $Co(OH)_2$ loadings have been prepared, and their electrocatalytic activity toward OER studied. The turnover frequency for O_2 evolution increases drastically as the amount of deposited hydroxide decreases. For FTO/$Fe(OH)_2$ electrodes, a maximum value close to 1 s^{-1} (at an overpotential of 0.47 V) has been determined for a coverage of 0.1 ML, remaining constant up to a coverage of around 3.5 ML. Beyond this point, a gradual decrease in the TOF values is observed. On the other hand, in the case of FTO/$Co(OH)_2$

electrodes, a coverage as low as 0.06 ML leads to a maximum TOF value of around 30 s^{-1} (at an overpotential of 0.47 V), while for higher coverages the TOF magnitude progressively decreases. In both cases, the hydroxide deposits leading to a maximum TOF value are formed by islands on the FTO substrate in which the amount of hydroxide directly exposed to both substrate and solution is maximum. This suggests that Fe and Co atoms far from the conducting substrate (thicker films) are less active for promoting OER due to the low intrinsic electrical conductivities of the studied hydroxides. Using a nanostructured substrate is therefore appealing as the fraction of deposited electrocatalyst in direct contact with the electrolyte would increase.

On the other hand, the high degree of control achieved with the CBD synthesis method can be used for the preparation of mixed layers (or bilayers) formed by hydroxides of two or three metals. Such a synthetic procedure allows to finely control the deposited amount of each hydroxide and the relative spatial arrangement of the different deposited layers and to finally study the effect of these variables on the final electrocatalytic response of the electrode. Experiments along these lines are currently underway in our laboratory.

Acknowledgements.

Financial support of the Spanish Ministry of Economy and Competitiveness through project MAT2015-71727-R (FONDOS FEDER) is gratefully acknowledged. J. Q. thanks to the Spanish Ministry of Education, Culture, and Sport (MECD) for the award of an FPU predoctoral grant (FPU15/02005). Dr. Teresa Lana-Villarreal is acknowledged for the acquisition and discussion of the Raman spectra.

References

[1] J. R. Mckone, N. S. Lewis, H. B. Gray, Chem. Mater. 2014, 26, 407–414.

[2] T. R. Cook, D. K. Dogutan, S. Y. Reece, Y. Surendranath, T. S. Teets, D. G. Nocera, Chem. Rev. 2010, 110, 6474–6502.

[3] N. S. Lewis, D. G. Nocera, Proc. Natl. Acad. Sci. 2006, 103, 15729–15735.

[4] M. G. Walter, E. L. Warren, J. R. McKone, S. W. Boettcher, Q. Mi, E. A. Santori, N. S. Lewis, Chem. Rev. 2010, 110, 6446–6473.

[5] H. Zhou, T. Fan, D. Zhang, ChemCatChem 2011, 3, 513–528.

[6] M. T. M. Koper, J. Electroanal. Chem. 2011, 660, 254–260.

[7] J. Rossmeisl, Z. W. Qu, H. Zhu, G. J. Kroes, J. K. Nørskov, J. Electroanal. Chem. 2007, 607, 83–89.

[8] S. Trasatti, G. Lodi, in: S. Trasatti (Ed.) Electrodes Conductive Metallic Oxides, Part B, Elsevier, Amsterdam, 1981.

[9] S. Trasatti, J. Electroanal. Chem. 1980, 111, 125–131.

[10] Y. Matsumoto, E. Sato, Mater. Chem. Phys. 1986, 14, 397–426.

[11] A. Di Blasi, C. D’Urso, V. Baglio, V. Antonucci, A. S. Arico’, R. Ornelas, F. Matteucci, G. Orozco, D. Beltran, Y. Meas, L. G. Arriaga, J. Appl. Electrochem. 2009, 39, 191–196.

[12] Y. Lee, J. Suntivich, K. J. May, E. E. Perry, Y. Shao-Horn, J. Phys. Chem. Lett. 2012, 3, 399–404.

[13] T. Reier, M. Oezaslan, P. Strasser, ACS Catal. 2012, 2, 1765–1772.

[14] E. Tsuji, A. Imanishi, K. I. Fukui, Y. Nakato, Electrochim. Acta 2011, 56, 2009–2016.

[15] Y. Gorlin, B. Lassalle-Kaiser, J. D. Benck, S. Gul, S. M. Webb, V. K. Yachandra, J. Yano, T. F. Jaramillo, J. Am. Chem. Soc. 2013, 135, 8525–8534.

[16] D. M. Robinson, Y. B. Go, M. Mui, G. Gardner, Z. Zhang, D. Mastrogiovanni, E. Garfunkel, J. Li, M. Greenblatt, G. C. Dismukes, J. Am. Chem. Soc. 2013, 135, 3494–3501.

[17] K. Mette, A. Bergmann, J.-P. Tessonnier, M. Hävecker, L. Yao, T. Ressler, R. Schlögl, P. Strasser, M. Behrens, ChemCatChem 2012, 4, 851–862.

[18] R. L. Doyle, M. E. G. Lyons, ECS Trans. 2013, 45, 3–19.

[19] M. E. G. Lyons, R. L. Doyle, M. P. Brandon, Phys. Chem. Chem. Phys. 2011, 13, 21530–21551.

[20] Y. Wu, M. Chen, Y. Han, H. Luo, X. Su, M. T. Zhang, X. Lin, J. Sun, L. Wang, L. Deng, W. Zhang, R. Cao, Angew. Chemie - Int. Ed. 2015, 54, 4870–4875.

[21] Y.-C. Liu, J. A. Koza, J. A. Switzer, Electrochim. Acta 2014, 140, 359–365.

[22] B. S. Yeo, A. T. Bell, J. Am. Chem. Soc. 2011, 133, 5587–5593.

[23] Y. Q. Gao, H. B. Li, G. W. Yang, J. Appl. Phys. 2016, 119, 34902.

[24] J. Liang, Y.-Z. Wang, C.-C. Wang, S.-Y. Lu, J. Mater. Chem. A 2016, 4, 9797–9806.

[25] D. Cibrev, M. Jankulovska, T. Lana-Villarreal, R. Gómez, Int. J. Hydrogen Energy 2013, 38, 2746–2753.

[26] X. Du, Y. Ding, C. Li, ChemCatChem 2015, 7, 2370–2376.

[27] C. Iwakura, A. Honji, H. Tamura, Electrochim. Acta 1981, 26, 1319–1326.

[28] R.-N. Singh, M. Hamdani, J.-F. Koenig, G. Poillerat, J. L. Gautier, P. Chartier, J. Appl. Electrochem. 1990, 20, 442–446.

[29] I. Nikolov, R. Darkaoui, E. Zhecheva, R. Stoyanova, N. Dimitrov, T. Vitanov, J. Electroanal. Chem. 1997, 429, 157–168.

[30] J. Suntivich, K. J. May, H. A. Gasteiger, J. B. Goodenough, Y. Shao-Horn, Science 2011, 334, 1383–1385.

[31] J. O'M. Bockris, T. Otagawa, J. Electrochem. Soc. 1984, 131, 290–302.

[32] J. O'M. Bockris, T. Otagawa, J. Phys. Chem. 1983, 87, 2960–2971.

[33] A. Singh, L. Spiccia, Coord. Chem. Rev. 2013, 257, 2607–2622.

[34] L. Trotochaud, S. W. Boettcher, Scr. Mater. 2014, 74, 25–32.

[35] J. R. Galán-Mascarós, ChemElectroChem 2015, 2, 37–50.

[36] D. S. Hall, D. J. Lockwood, C. Bock, B. R. MacDougall, Proc. R. Soc. A 2015, 471, 20140792.

[37] P. Oliva, J. Leonardi, J. F. Laurent, C. Delmas, J. J. Braconnier, M. Figlarz, F. Fievet, A. de Guibert, J. Power Sources 1982, 8, 229–255.

[38] J. R. S. Brownson, C. Lévy-Clément, Electrochim. Acta 2009, 54, 6637–6644.

[39] M. Dinamani, P. V. Kamath, J. Appl. Electrochem. 2000, 30, 1157–1161.

[40] X. Leng, K.-H. Wu, Q. Zeng, I. R. Gentle, D.-W. Wang, Asia-Pacific J. Chem. Eng. 2016, 11, 415–423.

[41] S. Zou, M. S. Burke, M. G. Kast, J. Fan, N. Danilovic, S. W. Boettcher, Chem. Mater. 2015, 27, 8011–8020.

[42] R. Subbaraman, D. Tripkovic, K.-C. Chang, D. Strmcnik, A. P. Paulikas, P. Hirunsit, M. Chan, J. Greeley, V. Stamenkovic, N. M. Markovic, Nat. Mater. 2012, 11, 550–557.

[43] L. Trotochaud, S. L. Young, J. K. Ranney, S. W. Boettcher, J. Am. Chem. Soc. 2014, 136, 6744–6753.

[44] A. M. Smith, L. Trotochaud, M. S. Burke, S. W. Boettcher, Chem. Commun. 2015, 51, 5261–5263.

[45] M. S. Burke, M. G. Kast, L. Trotochaud, A. M. Smith, S. W. Boettcher, J. Am. Chem. Soc. 2015, 137, 3638–3648.

[46] F. Dionigi, P. Strasser, Adv. Energy Mater. 2016, 6, 1600621.

[47] S. L. Candelaria, N. M. Bedford, T. J. Woehl, N. S. Rentz, A. R. Showalter, S. Pylypenko, B. A. Bunker, S. Lee, B. Reinhart, Y. Ren, S. P. Ertem, E. B. Coughlin, N. A. Sather, J. L. Horan, A. M. Herring, L. F. Greenlee, ACS Catal. 2017, 7, 365–379.

[48] M. Gong, Y. Li, H. Wang, Y. Liang, J. Z. Wu, J. Zhou, J. Wang, T. Regier, F. Wei, H. Dai, J. Am. Chem. Soc. 2013, 135, 8452–8455.

[49] H. Lin, Y. Zhang, G. Wang, J. B. Li, Front. Mater. Sci. 2012, 6, 142–148.

[50] S. Chen, J. Duan, M. Jaroniec, S. Z. Qiao, Angew. Chemie - Int. Ed. 2013, 52, 13567–13570.

[51] U. M. Patil, J. S. Sohn, S. B. Kulkarni, S. C. Lee, H. G. Park, K. V. Gurav, J. H. Kim, S. C. Jun, ACS Appl. Mater. Interfaces 2014, 6, 2450–2458.

[52] U. M. Patil, R. V. Ghorpade, M. S. Nam, A. C. Nalawade, S. Lee, H. Han, S. C. Jun, Sci. Rep. 2016, 6, 35490.

[53] H. D. Lutz, H. Möller, M. Schmidt, J. Mol. Str. 1994, 328, 121–132.

[54] A. P. Grosvenor, B. A. Kobe, M. C. Biesinger, N. S. McIntyre, Surf. Interface Anal. 2004, 36, 1564.

[55] M. C. Biesinger, B. P. Payne, A. P. Grosvenor, L. W. M. Lau, A. R. Gerson, R. S. C. Smart, Appl. Surf. Sci. 2011, 257, 2717–2730.

[56] S. C. Tang, S. Vongehr, Y. Wang, L. Chen, X. K. Meng, J. Solid State Chem. 2010, 183, 2166–2173.

[57] M. S. Burke, L. J. Enman, A. S. Batchellor, S. Zou, S. W. Boettcher, Chem. Mater. 2015, 27, 7549–7558.

[58] N.-T. Suen, S.-F. Hung, Q. Quan, N. Zhang, Y.-J. Xu, H. M. Chen, Chem. Soc. Rev. 2017, 46, 337–365.

[59] Z. P. Xu, H. C. Zeng, J. Mater. Chem. 1998, 8, 2499–2506.

[60] Y. Du, D. O’Hare, Particuology 2010, 8, 188–191.

[61] Z. A. Hu, Y. L. Xie, Y. X. Wang, L. J. Xie, G. R. Fu, X. Q. Jin, Z. Y. Zhang, Y. Y. Yang, H. Y. Wu, J. Phys. Chem. C 2009, 113, 12502–12508.

[62] M. A. Sayeed, T. Herd, A. P. O’Mullane, J. Mater. Chem. A 2016, 4,991–999.

[63] T. Xue, X. Wang, J. M. Lee, J. Power Sources 2012, 201, 382–386.

[64] A. Ramadoss, S. J. Kim, Electrochim. Acta 2014, 136, 105–111.

[65] U. M. Patil, S. C. Lee, J. S. Sohn, S. B. Kukarni, K. V. Gurav, J. J. Kim, S. Lee, S. C. Jun, Electrochim. Acta 2014, 129, 334–342.

[66] J. Yang, H. Liu, W. N. Martens, R. L. Frost, J. Phys. Chem. C 2010, 114, 111–119.

[67] C. Li, X. Zhang, K. Wang, H. Zhang, X. Sun, Y. Ma, RSC Adv. 2012, 201, 382–386.

[68] M. A. Ghanem, A. M. Al-Mayouf, P. Arunachalam, T. Abiti, Electrochim. Acta 2016, 207, 177–186.

[69] V. Gupta, S. Gupta, N. Miura, J. Power Sources 2008, 177, 685–689.

[70] F. Song, X. Hu, Nat. Commun. 2014, 5, 4477.

[71] H. Jin, S. Mao, G. Zhan, F. Xu, X. Bao, Y. Wang, J. Mater. Chem. A 2017, 5, 1078–1084.

[72] CRC Handbook of Chemistry and Physics 84th Edition (Ed.: D. R. Lide), CRC Press, Boca Raton, Florida, 2003.

[73] M. E. G. Lyons, M. P. Brandon, J. Electroanal. Chem. 2010, 641, 119–130.

[74] S. C. Petitto, M. A. Langell, J. Vac. Sci. Technol. A 2004, 22, 1690–1696.

[75] G. A. Carson, M. H. Nassir, M. A. Langell, J. Vac. Sci. Technol. A 1996, 14, 1637.

CAPTIONS FOR THE FIGURES

Figure 1. (a) XRD patterns for an $Fe(OH)_2$ film (deposition time: 2.5 hours, red line) on FTO, and for the bare FTO substrate (black line). (b) Fe 2*p* and (c) O 1*s* XPS spectra (red line) and corresponding deconvolutions (black line) for an $Fe(OH)_2$ film prepared for a deposition time of 2.5 hours. FESEM images corresponding to a top view of $Fe(OH)_2$ films on FTO for deposition times of (d) 20 min and (e) 2.5 hours.

Figure 2. Cyclic voltammograms (scan rate: $20\ mV\cdot s^{-1}$) for bare FTO (black line) and FTO/$Fe(OH)_2$ electrodes corresponding to deposition times of 20 min, 60 min and 80 min (red, green and blue line, respectively). Inset: detail of the voltammetric curves in the high potential region.

Figure 3. (a) Current density for the OER at 0.7 V for FTO/$Fe(OH)_2$ electrodes vs. the charge density for the oxidation of $Fe(OH)_2$. (b) Turnover frequency for the OER at 0.7 V for FTO/$Fe(OH)_2$ electrodes as a function of the charge density for the oxidation of $Fe(OH)_2$.

Figure 4. (a) XRD patterns for an α-$Co(OH)_2$ film (deposition time: 2.5 hours, red line) on FTO, and for the bare FTO substrate (black line). (b) Co 2*p* and (c) O 1*s* XPS spectra (red line) and corresponding deconvolutions (black line) for a $Co(OH)_2$ film prepared for a deposition time of 2.5 hours. FESEM images corresponding to a top view of $Co(OH)_2$ films on FTO, corresponding to deposition times of (d) 20 min and (e) 2.5 hours.

Figure 5. (a) Stabilized cyclic voltammogram for bare FTO (black line) and FTO/Co(OH)$_2$ electrodes corresponding to deposition times of 10, 30 and 50 min (red, green and blue lines, respectively). Detail of the voltammetric curves in the Co redox region for FTO/Co(OH)$_2$ electrodes corresponding to deposition times of (b) 10 and 30 min (red and green lines, respectively), and (c) 50 min. (d) Stabilized cyclic voltammograms for FTO/Co(OH)$_2$ electrodes corresponding to deposition times of 70 min, 90 min and 120 min (red, black and green lines, respectively). Scan rate in all cases: 20 mV·s^{-1}.

Figure 6. Log-log plot of the $q_{Co}^{rev}/q_{Co}^{total}$ ratio as a function of q_{Co}^{total}, measured for FTO/Co(OH)$_2$ electrodes prepared for different deposition times.

Figure 7. (a) Current density for the OER at 0.7 V for FTO/Co(OH)$_2$ electrodes *vs*. the charge density for the reversible oxidation of Co(OH)$_2$. (b) Turnover frequency for the OER at 0.7 V for FTO/Co(OH)$_2$ electrodes as a function of the charge density for the reversible oxidation of Co(OH)$_2$.

Fig. 8. *Quasi*-steady-state polarization curve for the OER recorded for FTO/Fe(OH)$_2$ (deposition time: 10 min, red line) and FTO/Co(OH)$_2$ (deposition time: 20 min, black line) electrodes.

Figure 9. Scheme illustrating the differences in electrocatalytic activity toward OER for different regions of the (a) Fe(OH)$_2$ and (b) Co(OH)$_2$ deposits. The small thickness of the deposits for short deposition times maximizes the interfacial area of the Fe(OH)$_2$ and Co(OH)$_2$ deposits and minimizes the inner regions, leading to the best TOF performance.

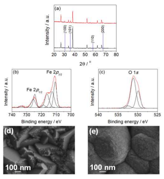
(a)
Intensity / a.u.
(100)
(101)
(110)
(200)
20
30
40
50
60
70
80
2θ / °
(b)
Fe 2$p_{3/2}$
Fe 2$p_{1/2}$
Intensity / a.u.
740
730
720
710
700
Binding energy / eV
(c)
O 1s
Intensity / a.u.
540
535
530
525
Binding energy / eV
(d)
100 nm
(e)
100 nm

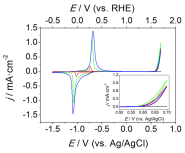
E / V (vs. RHE)
-0.5
0.0
0.5
1.0
1.5
2.0
1.5
1.0
0.5
0.0
-0.5
-1.0
-1.5
j / mA·cm^{-2}
-1.5
-1.0
-0.5
0.0
0.5
1.0
E / V (vs. Ag/AgCl)
1.2
0.9
0.6
0.3
0.0
j / mA·cm^{-2}
0.50
0.55
0.60
0.65
0.70
E / V (vs. Ag/AgCl)

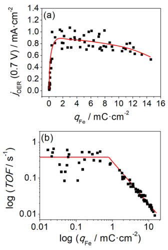
(a)
1.4
1.2
1.0
0.8
0.6
0.4
0.2
0.0
j_{OER} (0.7 V) / mA·cm^{-2}
0
2
4
6
8
10
12
14
16
q_{Fe} / mC·cm^{-2}
(b)
1
0.1
0.01
log (TOF / s^{-1})
0.01
0.1
1
10
log (q_{Fe} / mC·cm^{-2})

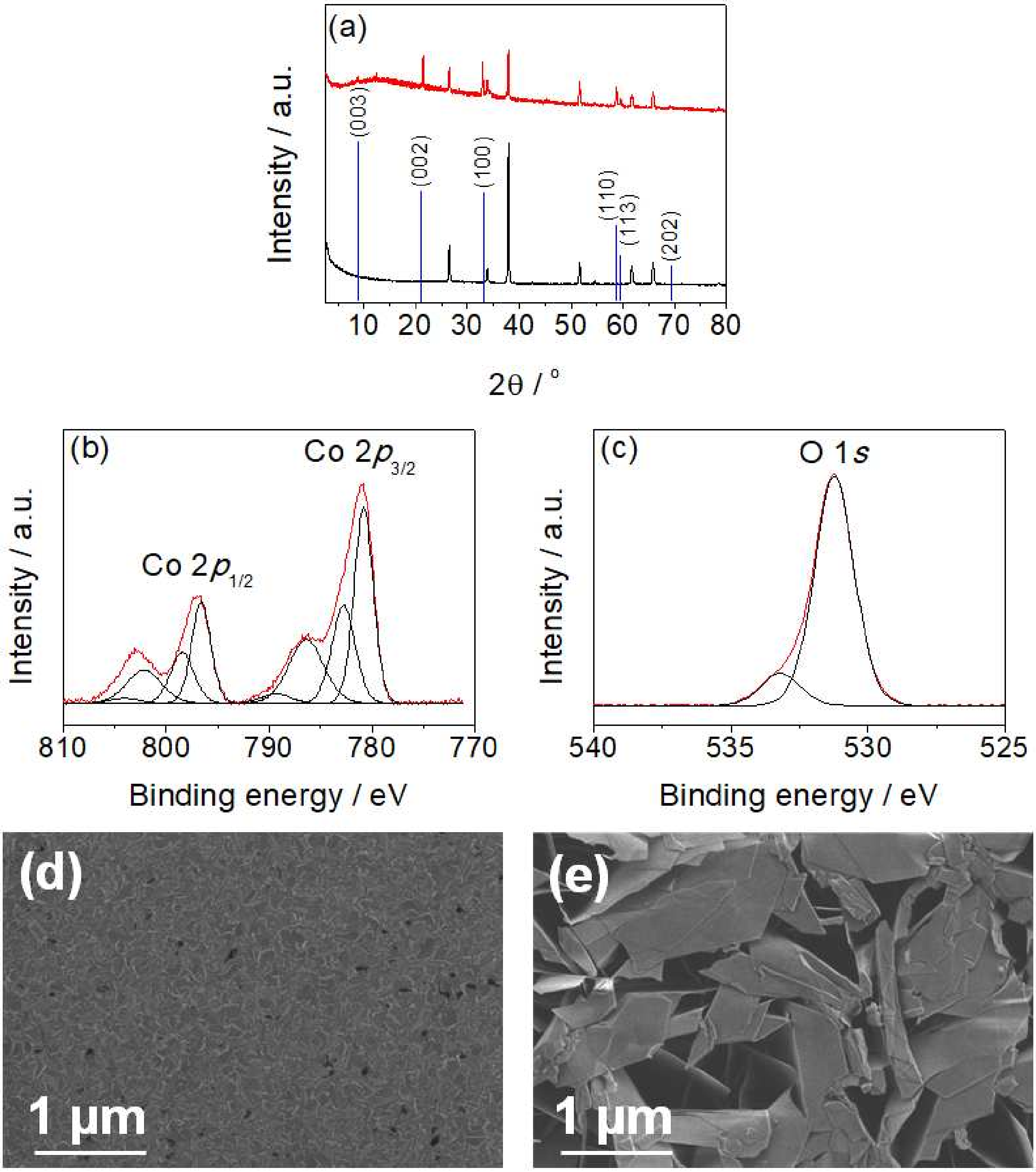
(a)
Intensity / a.u.
(003)
(002)
(100)
(110)
(113)
(202)
10
20
30
40
50
60
70
80
2θ / °
(b)
Co 2$p_{3/2}$
Co 2$p_{1/2}$
Intensity / a.u.
810
800
790
780
770
Binding energy / eV
(c)
O 1s
Intensity / a.u.
540
535
530
525
Binding energy / eV
(d)
1 µm
(e)
1 µm

AC

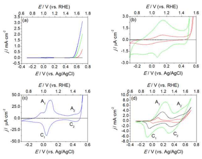
(a)
(b)
(c)
(d)
E / V (vs. RHE)
E / V (vs. Ag/AgCl)
j / mA·cm⁻²
j / μA·cm⁻²
A1
A2
C1
C2
0.6 0.8 1.0 1.2 1.4 1.6 1.8
-0.4 -0.2 0.0 0.2 0.4 0.6 0.8
-0.5 0.0 0.5 1.0 1.5 2.0 2.5 3.0 3.5
-3.0 -1.5 0.0 1.5 3.0
-50.0 -25.0 0.0 25.0 50.0
-8.0 -6.0 -4.0 -2.0 0.0 2.0 4.0 6.0 8.0 10.0

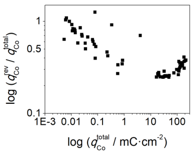
$\log (q_{Co}^{rev} / q_{Co}^{total})$
1
0.5
0.1
1E-3
0.01
0.1
1
10
100
$\log (q_{Co}^{total}$ / mC·cm^{-2})

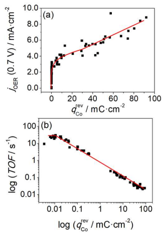
(a)
j_{OER} (0.7 V) / mA·cm^{-2}
10.0
8.0
6.0
4.0
2.0
0.0
0
20
40
60
80
100
q_{Co}^{rev} / mC·cm^{-2}
(b)
log (TOF / s^{-1})
100
10
1
0.1
0.01
0.01
0.1
1
10
100
log (q_{Co}^{rev} / mC·cm^{-2})

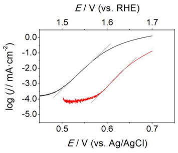
E / V (vs. RHE)
1.5
1.6
1.7
0.0
-1.0
-2.0
-3.0
-4.0
-5.0
log (*j* / mA·cm^{-2})
0.5
0.6
0.7
E / V (vs. Ag/AgCl)

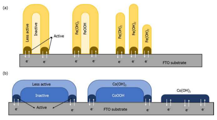
(a)
Less active
Inactive
Active
$Fe(OH)_2$
FeOOH
$Fe(OH)_2$
$Fe(OH)_2$
$Fe(OH)_2$
e^-
FTO substrate
(b)
Less active
Inactive
Active
$Co(OH)_2$
CoOOH
$Co(OH)_2$
e^-
FTO substrate

Highlights

- A urea-based bath allows to prepare transparent Fe and Co hydroxide electrodes.
- Conformal layers and nanoparticles appear respectively for Co and Fe hydroxides.
- Electrocatalyst loading is evaluated from the M(III)/M(II) surface process charge.
- The O_2-evolution turnover frequency is maximum for $M(OH)_2$ submonolayer loadings.